J Appl Electrochem (2014) 44:1007–1011
DOI 10.1007/s10800-014-0725-8

RESEARCH ARTICLE

High-efficiency photoelectrochemical performance of PbS nanoparticles sensitized TiO_2 nanotube arrays

Jianlei Qiao · Qingyao Wang · Yingkui Xiao

Received: 2 May 2014 / Accepted: 28 July 2014 / Published online: 17 August 2014

Abstract TiO_2 nanotube arrays sensitized by PbS nanoparticles (TiO_2 NTs/PbS) with enhanced visible-light activity were synthesized by a two-step approach including an electrochemical anodization technique followed by an in situ photodeposition approach. The structural investigations indicated that PbS nanoparticles grew uniformly on the walls of the TiO_2 NTs. The TiO_2 NTs/PbS exhibited more excellent photoelectrochemical properties than that of the TiO_2 NTs under visible-light irradiation. The enhanced photoelectrochemical activity of the TiO_2 NTs/PbS could be attributed to the improvement of visible-light absorption and charge separation derived from the coupling effect of the PbS nanoparticles and TiO_2 NTs.

Keywords TiO_2 nanotube arrays · PbS nanoparticles · Photodeposition · Photoelectrochemical activity

1 Introduction

Titanium dioxide nanotube arrays (TiO_2 NTs) have attracted great interest due to their unique electronic and optical properties, which can be applied in photocatalysis, biosensor, and photo-chromic devices, among other applications [1–4]. However, the large band gap of TiO_2 limits its photoactivity in the UV region of the solar spectrum. A clear way to enhance the efficiency of TiO_2 would be to extend its photoactivity to the visible region of the spectrum [5, 6]. The coupling of semiconductors with narrow band gap to TiO_2 NTs has been proved to be an efficient method to enhance the photoresponse to the visible-light region [7]. Lead sulfide (PbS) is an attractive semiconductor for this approach because of its small band gap (0.41 eV) and large exciton Bohr radius of 20 nm, which leads to extensive quantum size effects [8]. These specific advantages give more latitude to effectively use the size quantization effect for extending the absorption into the infrared range that comprises ~40 % of the solar spectrum.

In order to improve the separation of photogenerated charge carriers, PbS nanoparticles have been often combined with the TiO_2 NTs to form a heterojunction nanostructure. Craig A. Grimes and his colleagues [9] applied successive ionic layer adsorption and reaction and electrodeposition methods to synthesize PbS nanoparticles for sensitisation of the TiO_2 NTs. However, the reported photoconversion efficiency was still fairly low because of the poor combination of these two materials. Recently, we have newly developed simple and versatile low-temperature photodeposition techniques for directly coupling PbS nanoparticles on the surface of TiO_2 NTs by taking advantage of the photocatalysis and photoinduced surface superhydrophilicity. The application of in situ photodeposition deposition technique to sensitize TiO_2 NTs allows us to obtain two unique features: one is that efficient interfacial charge transfer is inherently guaranteed because TiO_2 photocatalysis is utilized, and the other is that a large amount of PbS nanoparticles can be deposited on not only the external surfaces but also the inner surfaces of the TiO_2

J. Qiao
College of Horticulture, Jilin Agricultural University, Changchun 130118, People's Republic of China

Q. Wang (✉)
School of Chemistry and Materials Science, Ludong University, Yantai 264025, People's Republic of China
e-mail: minli01@126.com; wangqingyao0532@163.com

Y. Xiao
Key Laboratory of Bionic Engineering (Ministry of Education), Jilin University, Changchun 130022, People's Republic of China

NTs [10]. Therefore, the photodeposition sensitisation of TiO_2 NTs with regulatable coverage of PbS nanoparticles is significative. In this paper, we demonstrated a photodeposition method for tethering PbS nanoparticles on the TiO_2 NTs to produce nanoscale heterostructures, and the prepared TiO_2 NTs/PbS exhibited an exceptionally high photoelectrochemical activity under visible-light irradiation.

2 Experimental

2.1 Preparation of PbS nanoparticles on the TiO_2 nanotube arrays

The TiO_2 NTs were prepared according to a two-step anodization, which was similar to our previous reports [11, 12]. PbS nanoparticles sensitized TiO_2 NTs photoelectrodes were successively prepared by photodeposition technique. Briefly, ethanol solution containing 2 mM $Pb(Ac)_2$ and 0.2 mM S was prepared under continuous stir and then the TiO_2 NTs substrate was immersed in the solution. After the solution had been bubbled with argon for 0.5 h in the dark, irradiation was carried out from the direction of the TiO_2 NTs with a 500 W Xe arc lamp for 30 min.

2.2 Characterization

The phase compositions of samples were determined by a Rigaku D/Max 2,400 X-ray diffractometer (XRD) equipped with graphite monochromatized Cu Kα radiation. The morphology of the prepared samples was observed using scanning electron microscopy (SEM, Quanta 200 FEG). UV–Vis diffuse reflectance spectra (DRS) of the samples were recorded on a UV-2,550 UV–Vis spectrophotometer with an integrating sphere attachment. Photoelectrochemical measurements were performed a mixture of 0.1 M Na_2S and 0.1 M Na_2SO_3 solution. The working electrode was illuminated with a solar simulator equipped with a 500 W Xe lamp with a visible-light filter (>420 nm). The photocurrent dynamics of the working electrode were recorded according to the responses to sudden switching on and off at 0.25 V bias.

2.3 Photocatalytic activity test

The photocatalytic activity of the prepared samples was evaluated by photocatalytic decomposition of MO solution under a 500 W Xe lamp with a visible-light filter (>420 nm) irradiation. Before photodegradation, adsorption equilibrium for the dye on catalyst surface was established by mechanical stirring in the dark for 30 min.

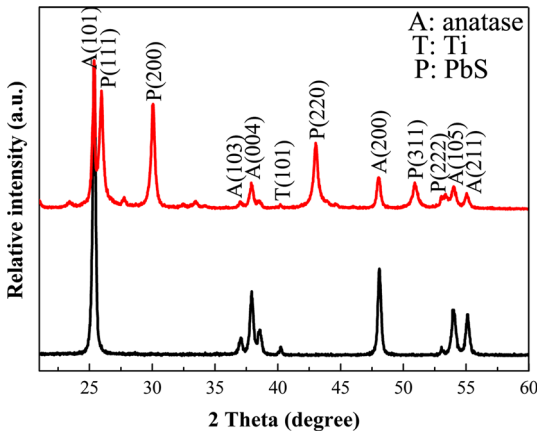

Fig. 1 XRD patterns of the TiO_2 NTs (*a*) and TiO_2 NTs/PbS (*b*)

After visible-light irradiation for 1 h, the remaining dye concentration was determined with a UV 1700 UV–Vis spectrophotometer by detecting the maximum absorption wavelength for MO at 464 nm.

3 Results and discussions

The typical XRD patterns of the TiO_2 NTs and TiO_2 NTs/PbS are shown in Fig. 1. The annealed TiO_2 NTs (Fig. 1a) demonstrated a distinct XRD pattern that confirmed the formation of anatase TiO_2 indexed to a standard JCPDS card (PDF no. 21–1272, labeled "A"). One could also observe the signals from the underlying Ti (PDF no. 44–1294, labeled "T"). The PbS sensitized TiO_2 NTs had single intensities *P* (1 1 1), *P* (2 0 0), *P* (2 2 0), *P* (3 1 1), and *P* (2 2 2) at 2θ values: 25.96°, 30.06°, 43.03°, 50.95°, and 53.39°, respectively, which indicated a cubic structure of PbS (PDF no. 65–0692, labeled "P"), indicating that PbS nanoparticles were deposited on the TiO_2 nanotubes.

Figure 2 showed the top-view and cross-sectional SEM images of the TiO_2 NTs and PbS-decorated TiO_2 NTs. From Fig. 2a and d, it was observed that the TiO_2 NTs had a regularly arranged pore structure. The TiO_2 NTs were entirely smooth with the same outer diameter of 160 nm. After photodeposition modification on the TiO_2 NTs, the tube walls became decorated with aggregates of fine PbS nanoparticles partly penetrating into TiO_2 NTs pores. The high-magnification SEM images (Fig. 2c, f) of the TiO_2 NTs/PbS showed the uniform aggradation of PbS nanoparticles with average diameter of 50 nm.

The UV–Vis DRS of the TiO_2 NTs and TiO_2 NTs/PbS are presented in Fig. 3. The absorption edge of pure TiO_2 NTs was observed at about 380 nm, corresponding to the band-gap energy of 3.2 eV. After photodeposition of PbS nanoparticles on the TiO_2 NTs, the sample exhibited an

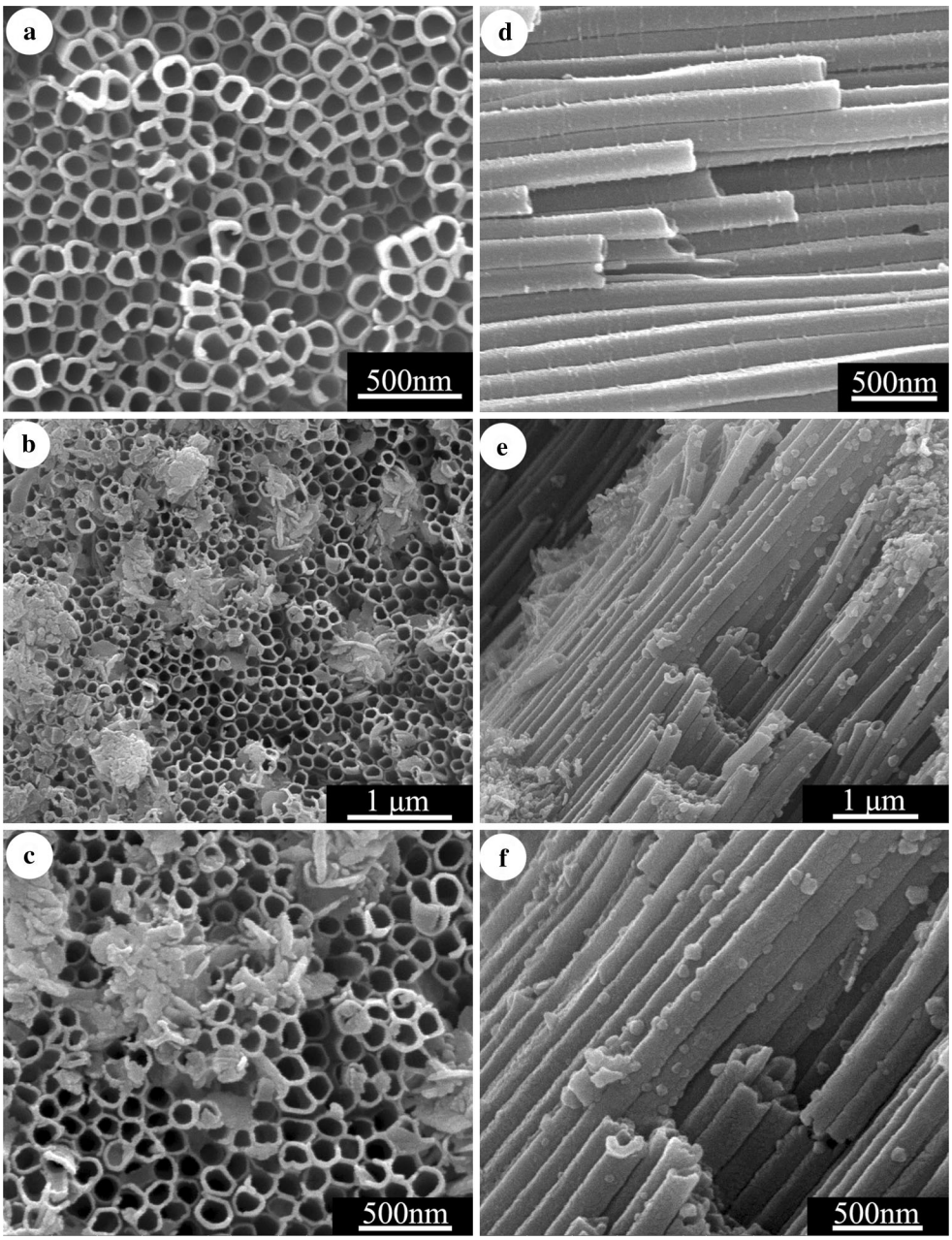

Fig. 2 SEM images of the TiO_2 NTs (**a** and **d**) and TiO_2 NTs/PbS (**b**, **c**, **e**, and **f**): top-view (**a–c**) and cross-sectional view (**d–f**)

obvious absorption in a wide wavelength range from UV to entire visible-light region. The enhanced ability of the TiO_2 NTs/PbS electrode to absorb visible light made it a promising solar cell and photocatalyst for solar-driven applications.

The transient photocurrent responses and current voltage (I–V) curves of the TiO_2 NTs and TiO_2 NTs/PbS were measured under visible-light irradiation, respectively. From Fig. 4a, it could be seen that the average photocurrent density of the TiO_2 NTs was nearly zero mA cm^{-2} because of none visible-light absorption, whereas that of TiO_2 NTs/PbS was 9.49 mA cm^{-2}. The photocurrent improvement of the TiO_2 NTs/PbS was mainly attributed to the PbS responsive to visible light. Meanwhile, I–V curves of the samples were further measured under visible-light irradiation (Fig. 4b), which further confirmed that the photocurrent density of the TiO_2 NTs/PbS was much higher than that of the plain TiO_2 NTs.

To evaluate the photocatalytic degradation capability of the TiO_2 NTs/PbS, we examined the decomposition of the dye MO under visible-light irradiation (Fig. 5a). The 88.7 % of MO removal was obtained after 4 h, while only

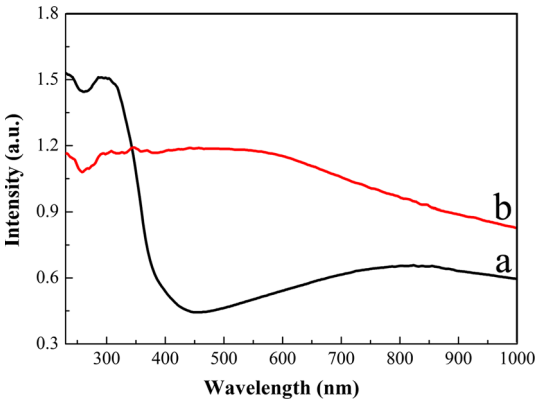

Fig. 3 UV–Vis spectra of the TiO_2 NTs (*a*) and TiO_2 NTs/PbS (*b*)

9.2 % of MO removal by TiO_2 NTs was obtained in the photocatalytic process with same irradiation time. The excellent performance of the TiO_2 NTs/PbS can be attributed to the interaction between PbS nanoparticles and TiO_2 NTs. The detailed photocatalytic progress could be inferred as following: when illuminated, PbS nanoparticles effectively absorb visible lights and excite electrons and holes pairs. Owning to the small size effect of the PbS nanoparticles, the conduction band (CB) of the PbS could be split, and the CB of the TiO_2 lays more positive than that of the PbS CB, then electron injection is expected from the photoexcited PbS nanoparticles into the TiO_2 CB [13]. Thus, the photogenerated electron–hole pairs are separated effectively by the *p–n* junction formed on the TiO_2 NTs/

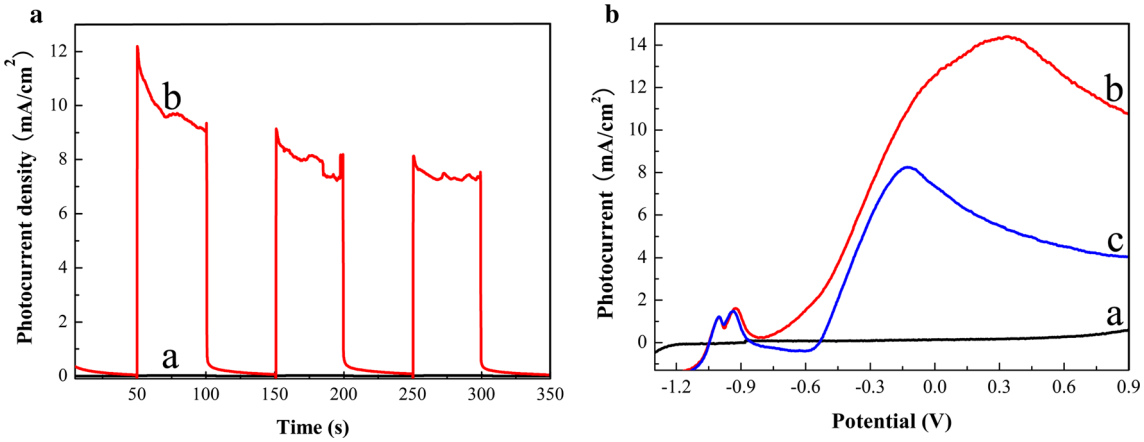

Fig. 4 The transient photocurrent (**a**) and I–V characteristics (**b**) of the samples under visible-light irradiation: TiO_2 NTs (*a*), TiO_2 NTs/PbS (*b*), and TiO_2 NTs/PbS in dark (*c*)

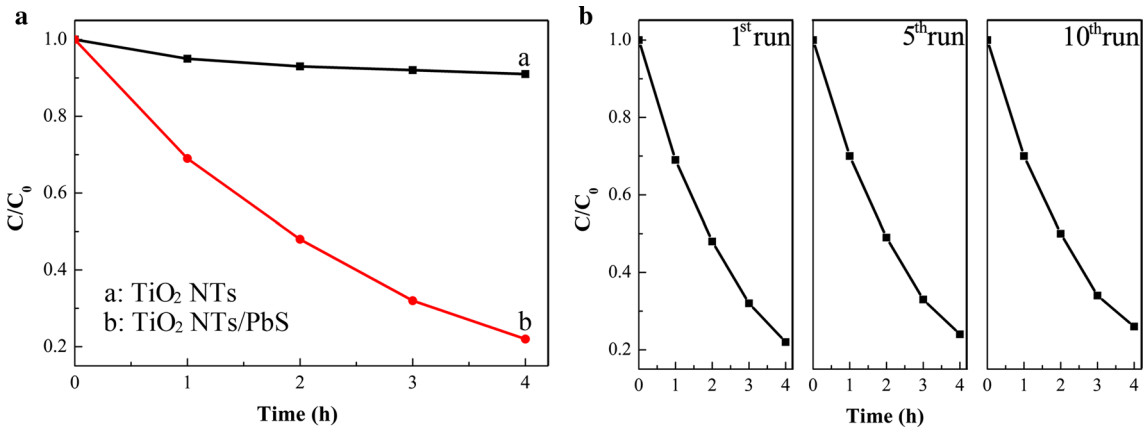

Fig. 5 The photocatalytic degradation of MO under visible-light irradiation (**a**): (curve *a*: TiO_2 NTs, curve *b*: TiO_2 NTs/PbS). Cycling degradation curves for the TiO_2 NTs/PbS (**b**)

PbS interface, and the recombination of electron–hole pairs can be reduced. The separated electrons and holes are then free to initiate reactions with the MO adsorbed on the photocatalyst surfaces. To investigate the photocatalytic stability of the TiO_2 NTs/PbS, five and ten cycles of photodegradation of MO (Fig. 5b) were conducted under visible-light irradiation. After the tenth runs, the degradation ratio of MO was well maintained, i.e., dropped only to 4.4 %, indicating that the TiO_2 NTs/PbS photocatalyst could be safely reused.

4 Conclusions

In summary, we have developed a simple photodeposition method to fabricate small and uniform PbS nanoparticles on the TiO_2 NTs. The sensitisation of the TiO_2 NTs by PbS nanoparticles significantly enhanced visible-light response of the electrode. The TiO_2 NTs/PbS showed higher photocurrents and consequently higher photocatalytic activity. The enhanced photoelectrochemical properties were attributed to the extended absorption in the entire visible-light region resulting from PbS nanoparticles, and the effective separation of photogenerated carriers driven by the photoinduced potential difference was generated at the interface of the TiO_2 NTs/PbS.

Acknowledgments This work was financially supported by the Science and Technology Development Project of Jilin Province (No. 20140520161JH).

References

1. Mirabolghasemi H, Liu N, Lee K, Schmuki P (2013) Chem Commun 49:2067–2069
2. Yu L, Wang ZY, Zhang L, Wu HB, Lou XW (2013) J Mater Chem A 1:122–127
3. Kuo YY, Li TH, Yao JN, Lin CY, Chien CH (2012) Electrochim Acta 78:236–243
4. Tsui LK, Homma T, Zangari G (2013) J Phys Chem C 117:6979–6989
5. Cai FG, Yang F, Xi JF, Jia YF, Cheng CH, Zhao Y (2013) Mater Lett 107:39–41
6. Wang XL, Zheng J, Sui XT, Xie H, Liu BS, Zhao XJ (2013) Dalton Trans 42:14726–14732
7. Li GS, Wu L, Li F, Xu PP, Zhang DQ, Li HX (2013) Nanoscale 5:2118–2125
8. Wang DF, Zhao HG, Wu NQ, El Khakani MA, Ma DL (2010) J Phys Chem Lett 1:1030–1035
9. Kang Q, Liu SH, Yang LX, Cai QY, Grimes CA (2011) ACS Appl Mater Interfaces 3:746–749
10. Fujii M, Nagasuna K, Fujishima M, Akita T, Tada H (2009) J Phys Chem C 113:16711–16716
11. Wang QY, Qiao JL, Gao SM (2014) Mater Lett 131:354–357
12. Wang QY, Qiao JL, Xu XH, Gao SM (2014) Mater Lett 131:135–137
13. Etgar L, Moehl T, Gabriel S, Hickey SG, Eychmüller A, Grätzel M (2012) ACS Nano 6:3092–3099